Spectral Analysis of Rocket Wake Flow–Jet Interaction by Means of High-speed Schlieren Imaging

Daniel Kirchheck[★], Dominik Saile[★], and Ali Gülhan[★]
[★]Deutsches Zentrum für Luft- und Raumfahrt (DLR) e. V.
Institute of Aerodynamics and Flow Technology, Supersonic and Hypersonic Technologies Department
Linder Höhe 1, 51147 Cologne, Germany
daniel.kirchheck@dlr.de · dominik.saile@dlr.de · ali.guelhan@dlr.de

Abstract

The wake flow field of a generic rocket launcher geometry at Mach 0.8, with a supersonic exhaust jet at stagnation conditions from 288 to 919 K was analyzed regarding its spectral content by means of high-speed Schlieren imaging and pressure measurements. The spectral analysis captured typical wake flow frequencies and their characteristic mode shape for the cross-flapping and swinging motion of the ambient shear layer at $\text{Sr}_D = 0.19$ and 0.35. At certain conditions, a strong amplification of the swinging motion was observed, which is probably governed by a coupling of the dynamic wake flow modes and the acoustic chamber properties.

1. Introduction

During the ascent, a rocket launcher is exposed to ever-changing environmental conditions. Correspondingly, the external flow constantly changes and so do loads imposed on the launch vehicle. This applies in particular to the afterbody of launch vehicles with a nozzle, subjected to the ambient flow.[2] The afterbody flow of a rocket launcher is similar to the flow around an axisymmetric *backward-facing step* (BFS). On average, the flow around a BFS forms a large scale annular recirculation region. That region is enclosed by the rockets base surface, the nozzle surface and the shear layers between the recirculation, the cold ambient flow and the hot exhaust stream. Furthermore, the flow in the base region is highly unsteady. Instationary effects within the subsonic recirculation region act on the surface of the nozzle and base plate, but also impose effects farther downstream on the shear layer of the jet. Thus, the structures in the base region are exposed to local pressure fluctuations, or in other words, to periodic loads. Moreover, in some cases, there might be a coupling between the downstream and the upstream effects.[5]

The reliable prediction of such highly transient load conditions is of great importance for the development of new components of future space transportation systems. For this reason, the subarea B of the *Collaborative Research Centre* (SFB) TRR40 is designated to investigate the base flow of rockets.[3] In that collaboration, experimental and numerical work is conducted in close cooperation between universities, public research institutions, and partners from the industry. The main objective of the collaboration is to provide flight-relevant data for a realistic modeling of the base flow effects. Over the past years, investigations by means of highly resolved flow simulations and wind tunnel experiments have been carried out by numerous different groups, including the research collaboration in the frame of the SFB-TRR40. Refer to Haidn et al. (2018)[3] for an overview on available literature. A wide Mach number range in the subsonic/transonic and supersonic/hypersonic regimes ($\text{Ma}_\infty = 0.5 \ldots 6.0$) has been investigated at free-stream Reynolds numbers of the order of 10^6 to 10^7 per meter. These parameters correspond to a typical trajectory of a launch system, such as the Ariane 5. Correspondingly, the geometric similarity is derived from that launcher. However, to capture the driving effects in a flight-realistic representation, more parameters have to be taken into account. Those are for example: the displacement effects of the rocket's exhaust jet, the temperature ratio between the external and internal flow, the shear layers of the detached base flow and the exhaust jet, and also the dynamic modes of the jet.

In some of the previous experimental studies, the exhaust jet is modeled with a sting, formed according to the shape of the jet. Obviously, this approach only considers the displacement effects and it neglects the dynamics due to the flow interaction effects. Consequently, the jet is included by other groups. It's conditions are simulated by heating the gas to total temperatures of up to 600 K, and/or using helium instead of air.[11] Since helium features a comparable heat capacity ratio to the typical combustion products of *liquid oxygen and hydrogen* (LOX/LH2), vacuum exit velocities up to 2500 m/s can be reached.

The goal of such an approach is to improve the similarity with the objective to gather more details on the imposing loads. The interaction of a cold ambient flow with a cold jet has been extensively investigated by Saile et al. (2019).[5,7–9] He finds a strong amplification of the base pressure and density gradient fluctuations for Mach 0.8.[5,8] This effect is associated with the extraordinary base flow dynamics in comparison to the other Mach number cases, which is described to be interrelated with the shedding of a vortex from the recirculation region.[9] Further, it is hypothesized that the strong amplification is the result of the resonating dynamics between the near-wake flow and the jet noise generation mechanism called screeching. In detail, evidence is found that the jet screech is in resonance with the swinging motion of the separated shear layer from the shoulder. In his recent work,[5] an attempt is made to transfer the findings above to the real flight and explain the significantly increased buffet loads of Ariane 5 in the subsonic flight regime. This was used as a starting point of the work at hand; however this time with a flight-realistic and hot exhaust jet in comparison to the cold jet. Investigations with a hot exhaust jet are practically non-existent since it requires actual hydrogen/oxygen combustion.

The current paper compares wake flow phenomena between cold plume interaction and hot plume interaction test cases, as well as the isolated ambient and exhaust flows. These were visualized by high-speed Schlieren imaging and post-processed using spectral decomposition methods of the two-dimensional density gradient fields. The results enable a comparison with previous findings in literature and lead the way for the design of future experiments in that field. The overarching goal hereby, was to further substantiate or clarify the hypothesis of jet screeching as being one of the driving mechanisms for rocket buffeting under dedicated flow conditions.

2. Experimental Setup and Methods

To investigate rocket base flow dynamics with regard to flow-flow-interaction between the ambient free stream and the propulsive jet, also referred to as the external and internal flows, the test object, an axisymmetric wind tunnel model, was located within the external wind tunnel flow. There it was supplied with the propulsive gas via its support structure. The internal flow was generated by expansion through the models thrust nozzle at the base of the generic rocket.

2.1 Hot Plume Testing Facility (HPTF)

The test setup was located within the *Vertical Wind Tunnel Test Section (VMK)* of the *German Aerospace Center (DLR)* in Cologne. It included the necessary infrastructure to generate the external flow as well as the internal cold flow condition from a connected high-pressure air vessel. For the hot flow condition, the VMK is connected to a controlled *Gaseous Hydrogen and Oxygen (GH2/GO2) Supply Facility*, which feeds the model internal combustion chamber, where realistic stagnation conditions were generated prior to expanding the combustion gases through the models thrust nozzle. The VMK, its GH2/GO2 supply facility, the respective feed system for the wind tunnel model adapter, and the wind tunnel model itself comprise the *Hot Plume Testing Facility (HPTF)* of the DLR (Figure 1). It's main components and the details of the test setup are described in the following sections.

Vertical Wind Tunnel Test Section Cologne (VMK) The VMK is a blow-down type wind tunnel with an atmospheric free stream test section in vertical alignment. The maximum operating pressure is 35 bar, which is maintained by a pressure reservoir of 1,000 cubic meters volume at a maximum pressure of 67 bar. The schematical layout of the VMK is shown in Fig. 2(a). The reservoir allows typical test durations of 30 to 60 seconds and the upstream heat storage allows the flow to heat-up to 750 Kelvin, which enables testing at ground-level conditions up to a Mach number of 2.8. The flow Mach number is set by various discrete nozzles in the supersonic range up to Mach 3.2. Subsonic conditions are set by a convergent nozzle of 340 millimeter exit diameter. The detailed operating range is given in Fig. 2(b). The model extension is held by a central upstream support, which is integrated into the low-speed section of the subsonic nozzle and followed by two planes of metallic filter screens. The design of the test chamber is explosion proof and in combination with modern gas monitoring devices, explosion protected electric installations, and gas proof interfaces suitable for the operation of combustion tests with gaseous and solid propellant combinations. For the cold gas interaction tests, a high-pressure dried air supply is available with a maximum supply pressure of 150 bar.

GH2/GO2 Supply Facility The GH2/GO2 supply facility is an extension of the VMK infrastructure, which is designed especially for the hot gas investigations in the VMK test environment. It consists of a 300 bar gas storage for the supply with process gases (hydrogen, oxygen, and nitrogen for purging and inerting purposes) and a control station to set the operating conditions by an integrated mass flow controller. The control station operates at 130 bar and feeds the model combustor with a maximum of 399 g/s oxygen and 67 g/s hydrogen at a maximum chamber pressure of 115 bar (reference condition RC2). The resulting operating range as a function of chamber pressure p_{cc} and oxidizer–fuel–ratio
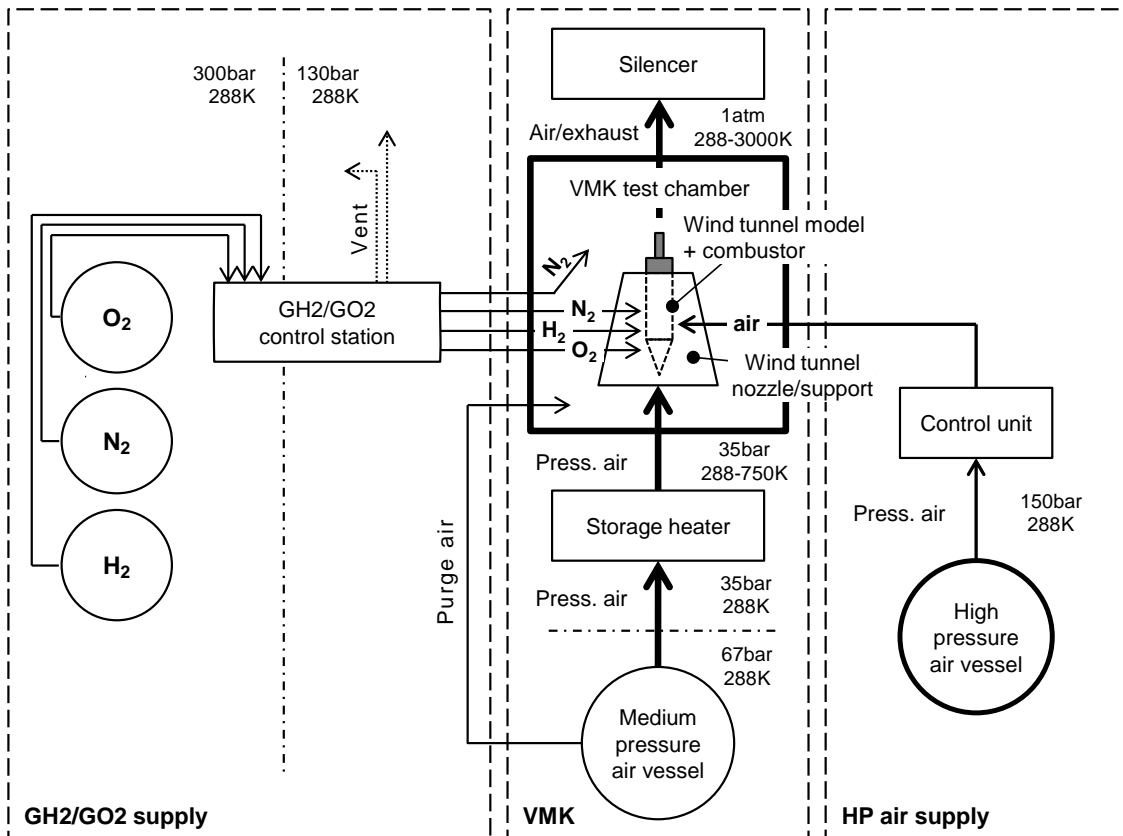
Figure 1: Schematic of the Hot Plume Testing Facility (HPTF), incorporating the Vertical Wind Tunnel Test Section (VMK), the GH2/GO2 supply facility, high-pressure air supply, and the test chamber, housing the wind tunnel nozzle, wind tunnel model adapter and wind tunnel model extension, including the GH2/GO2 combustor
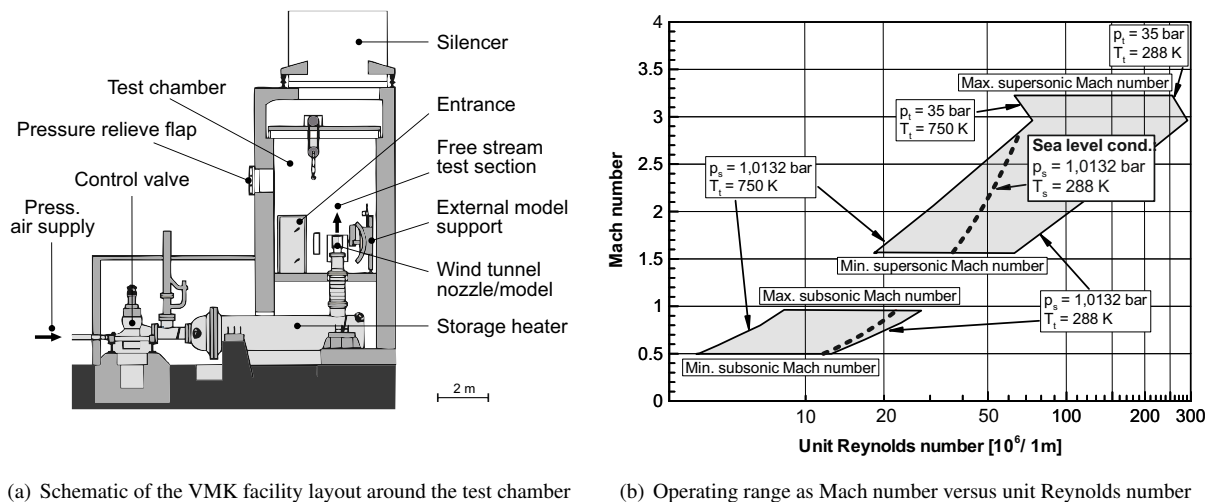
(a) Schematic of the VMK facility layout around the test chamber

(b) Operating range as Mach number versus unit Reynolds number

Figure 2: Vertical Wind Tunnel Test Section Cologne (VMK)

OFR is given in Fig. 3 as iso-contours of the theoretical chamber temperature T_{cc} (——) and the area specific mass flow rate $\dot{m}/A_{th}$ (------). The theoretical maximum operating envelope (——) and the model design envelope (filled area) are given by the maximum supply pressure/model design pressure, min./max. mass flow rates, the theoretical ignition limit at OFR > 0.5 and the maximum mass flow ratio OFR < OFR_{st} = 7.918.

3
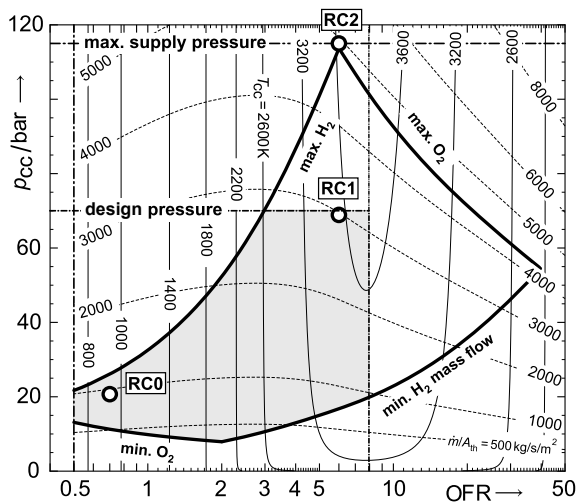
Figure 3: Operating range of the GH2/GO2 supply facility with reference conditions RC0, RC1, and RC2
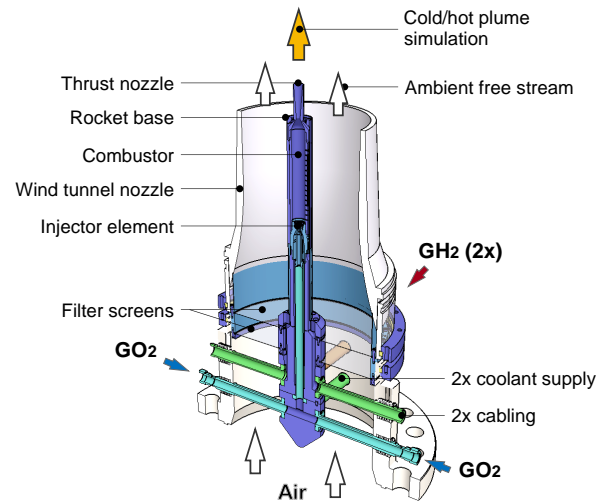
Figure 4: Wind tunnel nozzle with central upstream support, feed lines, and wind tunnel model extension

2.2 Wind Tunnel Model

The wind tunnel model is located on top of the central support structure, which is held within a cylindrical duct upstream of the convergent subsonic wind tunnel nozzle via eight tubes. They were used at the same time for supplying the model with combustion gases (2xGH2, 2xGO2) or high-pressure air, cabling for sensors and ignition, and optional coolant mass flow (Fig. 4). The detailed internal and external dimensions of the wind tunnel model extension are given in Fig. 5. The axisymmetric backward-facing step was a generic representation of the Ariane 5 main stage afterbody with respect to the ratios of L/D and d/D on a scale of $1/80$. The outer dimensions were equal to previous investigations by Saile et al. (2019),[5,7,8] although the model was remade due to the functional requirements for hot gas testing. The inner geometry of the thrust chamber and single element shear flow injector was designed and investigated in previous work.[6] The thrust chamber and nozzle extension were made of *oxygen-free high thermal conductivity (OFHC)* copper, the injector part was made by additive manufacturing of an Inconel 718 alloy with a maximum temperature rating of 1020 K to prevent hydrogen environment embrittlement.

2.3 Instrumentation and Diagnostic Methods

Ambient flow properties The characterization of the external flow was done by Pitot probe measurements with an additional static pressure port in the exit plane of the wind tunnel nozzle, approx. 11 mm upstream of the rocket base shoulder. It was used in a closed control loop for the setup of predefined ambient flow Mach numbers. The static free stream temperature for Mach number calculation was derived from isentropic relations, based on the total temperature inside the reservoir.

Combustor outflow properties The combustor outflow properties were characterized by static and dynamic pressure measurements of the total chamber pressure. The chamber pressure was extracted from the base plate next to the injector outlet at the locations PI1 with a certain transmission length l_{trans} and PS1 as a static reference measurement without temperature influences at $l_{\text{trans}} > 1$ m. The unsteady pressure signals were analyzed regarding their spectral content to characterize the input conditions to the wake flow dynamics. All measurement data was acquired at 10 kHz. Fast Fourier Transformation (FFT) of the pressure signals were performed to obtain the power spectra S_{xx} for an evaluation time window of 2 s at 10 Hz frequency resolution. Further, a Hanning window with an overlap of 50% and arithmetic amplitude averaging was used. The controlled mass flows of oxygen and hydrogen were measured at the control station via Coriolis flow meters. The sensor locations in cylindrical coordinates with respect to the center of the chamber base plate is given in Tab. 1, together with their respective nomenclature.

Flow visualization and spectral analysis The present work shows our first approach of visualizing the flow topology for both, the cold plume and GH2/GO2 hot plume test cases in combination with ambient flow. For that, a Schlieren optics setup with high-speed imaging equipment within the topological region given in Fig. 6 was used. The recording
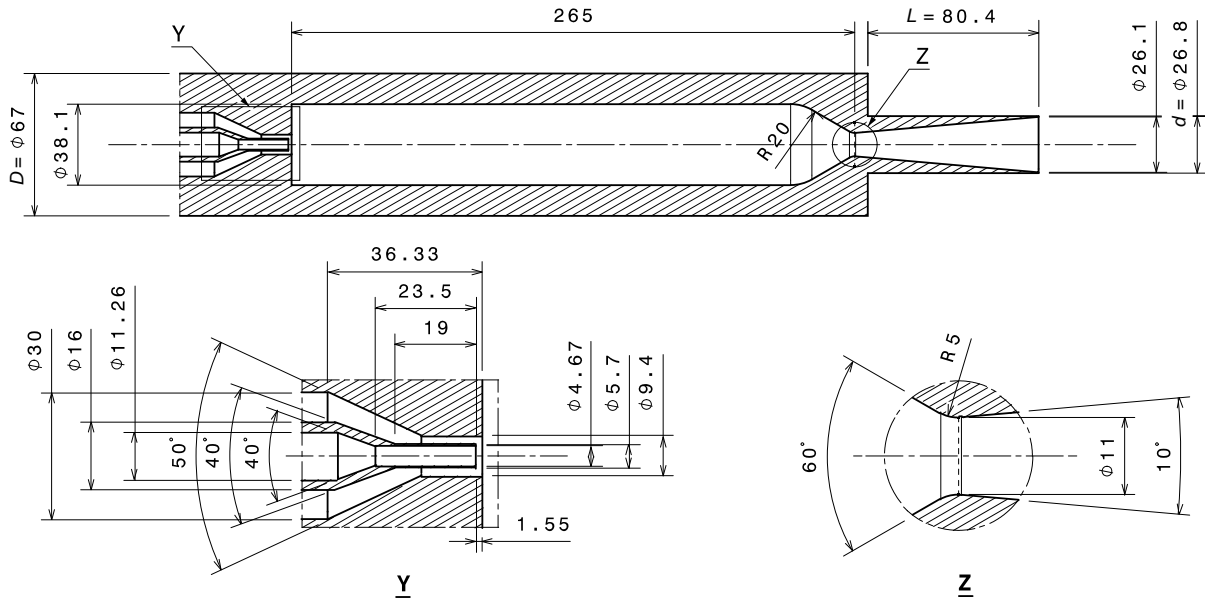
Figure 5: Internal and external dimensions of the wind tunnel model extension, including the cylindrical thrust chamber; Y: single element coaxial shear injector with O2 in the inner and H2 in the annular pipe; Z: nozzle throat section

Table 1: Combustion chamber instrumentation – sensor locations, type and nomenclature

ID	Sensing task	Sensor type	x/mm	r/mm	ϕ/°	l_{trans}/mm
PS1	Steady chamber pressure	Kulite XTEH-7L-190M-50BARA	0.00	16.00	-10	52.77
PI1	Unsteady chamber pressure	Kulite XCE-062-30BARA	0.00	16.00	10	> 1000

frequency was 20 kHz with a shutter speed of 2.5 μs. The goal was to analyze the Schlieren recordings with respect to their spectral content in order to identify and compare dominant frequencies, their intensities, and the local distribution in the wake between the different test cases. This was done by extracting the greyscale values of the images at specific image coordinates $I(x_{\text{px}}, y_{\text{px}})$ with I in $[0, 256]$ over time and performing an FFT of the time-resolved intensity fluctuations to obtain the power spectra. The FFT incorporated a 10 Hz frequency resolution with an overlap of 50 %. The investigated signal had a real time length of 0.5 s, consisting of 10,000 samples.

For a first global analysis, the amplitude spectra were spatially averaged within each frame, to easily identify the predominant frequencies. To further analyze the two-dimensional distribution of the mean fluctuation amplitude and the dominant frequencies in the field, the results were plotted as spatial distribution at certain isolated frequencies in the image coordinate system.

2.4 Test Matrix and Test Conditions

The present work compares three main test cases at the critical ambient flow Mach number of 0.8 to investigate the main characteristics of the base flow dynamics and topological features with regard to the influence of a hot exhaust jet. First, the cold exhaust jet is measured without ambient flow (V087) and the wake flow is measured without an active exhaust jet (V099). The latter is broadly known in literature as an axisymmetric backward facing step flow and offers numerous validation sources. Then, a cold exhaust jet is added to this configuration (V098) which is then comparable to the preceding investigations of Saile et. al.[5,8] Finally, the provided evaluation methods will be transferred to the case with a hot exhaust jet (V097). The first approach is to consequently keep the ambient flow and chamber conditions constant through all tests, as far as possible. The detailed test conditions are given in Tab. 2.

2.5 Assessment of the Estimated Dominant Frequencies

The findings from the spectral analysis were compared to typical dominant frequencies of specific types of flow features similar to, or included in, the flows under investigation. They were categorized in the acoustic and spatial modes of the models pressure chamber, modes of the dynamic motion of the rocket wake flow, and acoustic phenomena from the jet
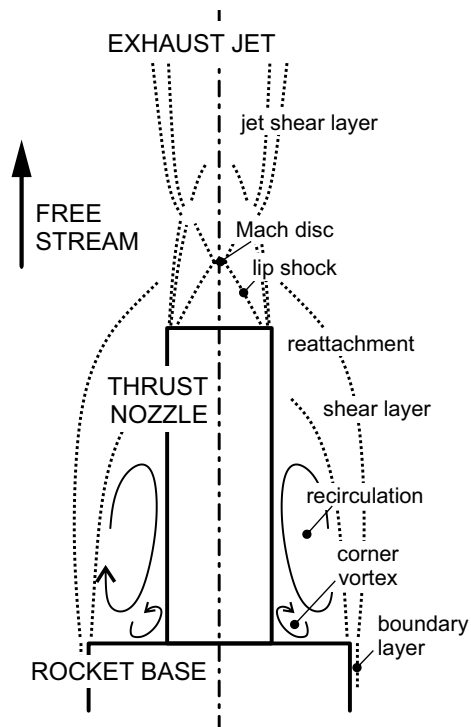
Figure 6: Typical topology of rocket base flow with an over-expanded exhaust jet and a thrust nozzle, exposed to the ambient reattaching shear layer

Table 2: Test matrix and test conditions

ID	Jet flow	Ma_∞	p_∞ bar	T_∞ K	p_{cc} bar	T_{cc} K	a_{cc} m/s	$\dot{m}_{cc}$ g/s	OFR	u_e m/s
V087	Cold jet (only)	–	1.019	255.4*	19.17	288.0*	334.8*	459.9*	–	619.8*
V099	No jet	0.80	0.981	255.4*	–	–	–	–	–	
V098	Cold jet	0.80	0.987	255.4*	19.90	288.0*	334.8*	459.9*	–	619.8*
V097	Hot jet	0.80	0.992	255.4*	20.27	918.7*	1750.6*	89.40	0.693	2803.9*

* From one-dimensional analysis; $T_{amb} \approx 288\,K$

dynamics. In the following paragraphs, formula for estimation are given and the resulting frequencies for the present test cases are listed in Tab. 3.

Model pressure chamber   As acoustic and spatial modes of the models pressure chamber, the Helmholtz mode, first and second logitudinal, as well as first tangential and radial modes were estimated. For the estimation of the Helmholtz mode (1) a mouth correction $\pi\bar{R}/2$ was used, where $\bar{R}$ (mouth radius) and $\bar{A}$ (mouth cross-sectional are) are given by the intermediate diameter $\bar{d} = (d_{\mathrm{th}} + d_{\mathrm{e}})/2$ of the conical nozzle with length $l \approx 90\,\mathrm{mm}$. For the chamber length, the distance at the middle of the convergent nozzle section was taken into account as $L_{\mathrm{cc}} \approx 255\,\mathrm{mm}$.

$$\text{Helmholtz mode,} \qquad f_{\mathrm{HH}} = \frac{a_{\mathrm{cc}}}{2\pi} \sqrt{\frac{\bar{A}}{V_{\mathrm{cc}}\left(l + \frac{\pi\bar{R}}{2}\right)}} \tag{1}$$

The frequencies for isolated and combined spatial modes were estimated from (2) and (3). Their mode numbers λ, τ, and ρ specify the rank of longitudinal, tangential, and radial modes respectively and the corresponding mode coefficient $\alpha_{\tau\rho}$, taken from Blomshield (2007),[1] was used for the calculation of combined tangential and radial modes.

$$\text{Spatial modes,} \qquad f_{\lambda\mathrm{L}\tau\mathrm{T}\rho\mathrm{R}} = \sqrt{f_\lambda^2 + f_{\tau\rho}^2} \tag{2}$$

$$f_\lambda = \frac{\lambda a_{\mathrm{cc}}}{2L_{\mathrm{cc}}}, \qquad f_{\tau\rho} = \frac{\alpha_{\tau\rho} a_{\mathrm{cc}}}{\pi D_{\mathrm{cc}}} \tag{3}$$

Wake flow dynamics   For the wake flow dynamics, it is common that characteristic dominant modes can be described by the non-dimensional Strouhal number Sr based on the main diameter D (4). High fidelity CFD computations using a zonal RANS/LES approach of a similar flow field with cold exhaust jet by Statnikov et al. (2017)[10] were taken as reference for these characteristic non-dimensional frequencies. They are reported as cross-pumping motion at $\mathrm{Sr}_D = 0.1$, cross-flapping motion at $\mathrm{Sr}_D = 0.2$ and swinging motion at $\mathrm{Sr}_D = 0.35$. The frequencies of the cross-flapping and swinging motion have also been confirmed by Saile et al. (2019)[7,8] using dynamic pressure measurements on the base of a generic rocket launcher geometry, which was the predecessor of the current test setup.

$$\text{Strouhal number,} \qquad \mathrm{Sr}_D = \frac{u_\infty f}{D}. \tag{4}$$

Jet dynamics   Regarding the dynamic features of a supersonic jet, screeching is also reported in related work by Saile et al. (2019)[5,8] as a possible driving mechanism for increased loads through an interaction with the incoming shear flow dynamics, if the respective frequencies are matching for a certain flow configuration. The jet screeching frequency was estimated from (5) with the weighted convective velocity of disturbances within the jet shear layer $u_{\mathrm{conv}} = 0.7\,(u_{\mathrm{e}} - u_\infty) + u_\infty$, the effective nozzle exit velocity u_{e}, and the length of the first shock cell of the supersonic jet L_{cell}, which was measured from the Schlieren images as $L_{\mathrm{cell}} = 45\,mm$ (V098) and $L_{\mathrm{cell}} = 46\,mm$ (V097).

Table 3: Expected frequencies from external and internal flow dynamics and acoustics

	Symbol	Cold jet	Hot jet	Unit	Reference
Model pressure chamber					
Helmholtz mode	f_{HH}	158.9	830.7	Hz	
First longitudinal mode	f_{1L}	656.5	3 432.5	Hz	[1]
Second longitudinal mode	f_{2L}	1 312.9	6 865.1	Hz	[1]
First tangential mode	f_{1T}	5 158.2	26 971.2	Hz	[1]
First radial mode	f_{1R}	10 720.6	56 056.0	Hz	[1]
Wake flow dynamics					
Cross-pumping motion	$f_{\mathrm{cp}} = f(\mathrm{Sr}_D = 0.1)$	376.5	376.5	Hz	[10]
Cross-flapping motion	$f_{\mathrm{cf}} = f(\mathrm{Sr}_D = 0.2)$	752.9	752.9	Hz	[10]
Swinging motion	$f_{\mathrm{sw}} = f(\mathrm{Sr}_D = 0.35)$	1 317.6	1 317.6	Hz	[10]
Jet dynamics					
Screeching	f_{sc}	1 246.9	1 329.7	Hz	[5,8]

SPECTRAL ANALYSIS OF ROCKET WAKE FLOW–JET INTERACTION

Refer to Saile (2019)[5] for a detailed summary on the jet screeching phenomenon in combination with ambient flow.

$$\text{Screeching frequency,} \qquad f_{\text{sc}} = \frac{u_{\text{conv}}}{L_{\text{cell}} \left(1 + \frac{u_{\text{conv}}}{a_\infty - u_\infty} \right)} \qquad (5)$$

The estimated frequencies for the given flow configurations are listen in Tab. 3. A comparison of the various frequencies for the two test cases with cold plume and hot plume interaction, revealed that the swinging motion of the ambient shear layer and the jet screeching frequencies were lying close to each other (f_{sw} = 1318 Hz, $f_{\text{sc,c}}$ = 1247 Hz, $f_{\text{sc,h}}$ = 1330 Hz). Considering that turbulent structures in the jet shear layer and fluctuating chamber conditions can lead to a variation of the convection velocity u_{conv}, the screeching frequency also varies, thus overlap of the spectral content was expected. Further, for the cold jet interaction, also the second longitudinal mode f_{1L} = 1313 Hz of the pressure chamber matched the swinging motion frequency. Thus, another influencing mechanism could lie in an interaction of the fluctuating jet shear layer and the periodical motion of the ambient shear layer, if the ambient shear layer attaches on the jet and the chamber conditions are fluctuating due to its acoustic properties.

3. Experimental Results

In the following section, it is shown that in case of cold jet interaction, where the swinging motion matched the jet screeching frequency on the one hand and the 2L mode of the pressure chamber on the other hand, large fluctuations arose within the wake flow region. In contrast, this was not the case for the hot jet interaction experiments. Therefore, the analysis of the results focuses on the causalities and evaluates the different influences on the wake flow dynamics.

3.1 Properties and Topological Features of the Mean Flow

The data was analyzed for steady state input conditions. Reaching a steady state took the longest for the combustion chamber, which is shown in Fig. 7. The combustion chamber pressure was considered constant after 20s. Correspondingly, all mean flow quantities given in Tab. 2 refer to a common evaluation time window at t_{eval} = [18, 20] s, in which the flow conditions were maintained constant with acceptable deviations of the mean values. The steady state of the chamber pressure for the hot test case (V097) at a controlled mass flow rate with constant set point values indicates that a thermal equilibrium could be reached with consequently constant chamber temperatures. Under these conditions, it is assumed that the one-dimensional equilibrium calculations for additional chamber properties (Tab. 2) are valid within an acceptable margin.

The averaged Schlieren images (Fig. 8) give information about the mean flow topology. The density gradients show the shear layer evolving from the base plate, which allowed a qualitative evaluation of the reattachment length of the ambient shear layer. It seems that in relation to the ambient flow without jet (V099), the reattachment length is reduced in case of cold jet interaction (V098). In case of the hot jet interaction (V097), it is apparently the opposite. The reduction of the reattachment length for the cold jet (V098) is as expected due to the suction effect of the jet. For the hot jet (V097), an even stronger suction effect is expected due to the higher jet velocity. Nevertheless, the
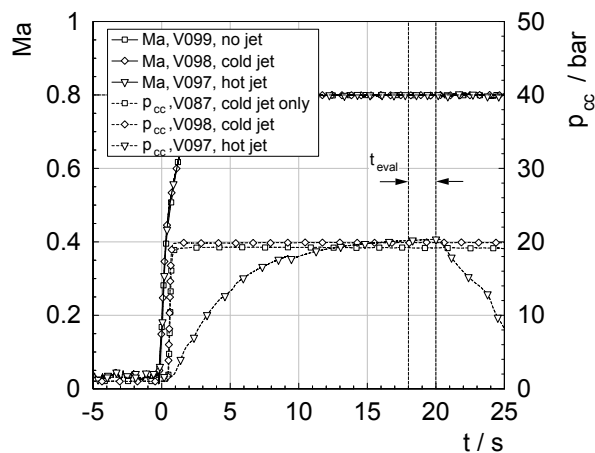
Figure 7: Major internal and external flow properties for all test cases in time; constant flow conditions are maintained within the evaluation time window at t_{eval} = [18.0, 20.0] s

(a) ambient flow, no jet (V099)   (b) cold jet only (V087)   (c) ambient flow, cold jet (V098)   (d) ambient flow, hot jet (V097)
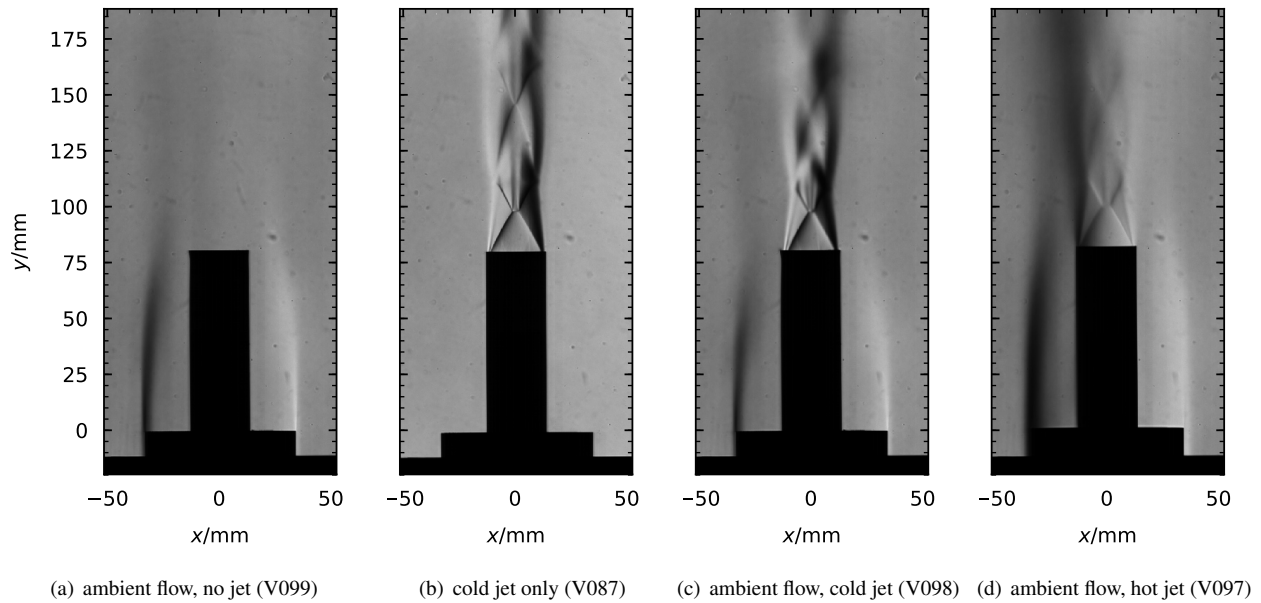
Figure 8: Averaged Schlieren images

contrary can be noted, which is why more data is necessary for clarification at another point in time. Note that Saile et al. (2019)[9] describe the reattachment location as being one possible driving parameter for the wake flow dynamics. Further, it is found that the excitation of the shear layer instabilities is largest when reattachment takes place at the nozzle tip.

3.2 Spectral Content of the Internal and External Flows

The power spectra of the dynamic total pressure measurements inside the model pressure chamber are shown in Fig. 9–11 for the ambient flow cases without jet, with cold jet, and with hot jet respectively. These were analyzed in combination with the spatial average of the intensity spectra from the HSS images, which is shown in the following paragraphs.

Ambient flow without jet   The power spectrum of the ambient flow case without jet (Fig. 9) shows five major peaks which are marked on the graph. According to Tab. 3, the peaks at 760 Hz and 1330 Hz can be clearly assigned to the cross-flapping and swinging motion frequencies of the shear layer, estimated as $f_{cf} = 753$ Hz and $f_{sw} = 1318$ Hz (Tab. 3), whereas the energy content of the swinging motion was almost one order of magnitude larger. Since the periodic flow movement at the tip of the nozzle obviously caused pressure fluctuations in the chamber, the Helmholtz mode ($f_{HH} = 159\,Hz$) was also excited, which is indicated by the peak at 160 Hz. For the two peaks at 50 Hz and 1590 Hz, no definite explanation is known to the author at the time of writing.

In the amplitude spectrum of the HSS images intensity fluctuations (Fig. 12), a dominant contribution is also visible in the range of 1290 Hz to 1360 Hz, which might as well trace back to the swinging motion of the shear layer. Another peak at 700 Hz gives an indication for an occurrence of the cross-flapping motion, although the frequency range does not match perfectly to the content in the power spectrum of the chamber pressure measurements. Possibly, this phenomenon is due to a frequency shift of the sound waves, being generated inside of a moving surrounding gas and traveling into a static gas volume in the chamber. Under this assumption, the motion of the wake would appear as $Sr_D (700\,Hz) \approx 0.19$, which is no major contradiction in relation to the estimated frequencies of the ambient flow without jet, since various influencing factors, which were not taken into account could modify the wake modes frequencies.

Ambient flow with cold jet   Next in Fig. 10, the spectra of the cold jet are discussed by switching on and off corresponding flow features. For the isolated cold jet, clustered peaks in the range of 630–750 Hz and around 1330 Hz can clearly be assigned to the first and second longitudinal mode of the pressure chamber. They are predicted as $f_{1L} = 657$ Hz and $f_{2L} = 1313$ Hz (3). The spectral shape of these peaks is broadband, which is reasonable due to the

SPECTRAL ANALYSIS OF ROCKET WAKE FLOW–JET INTERACTION
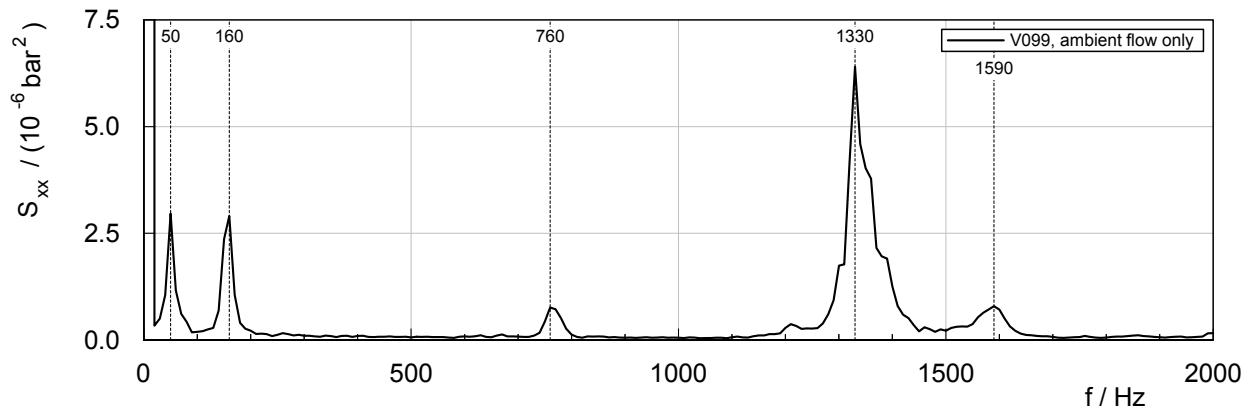
Figure 9: Power spectrum of the combustion chamber pressure signal for the ambient flow case without jet (V099)
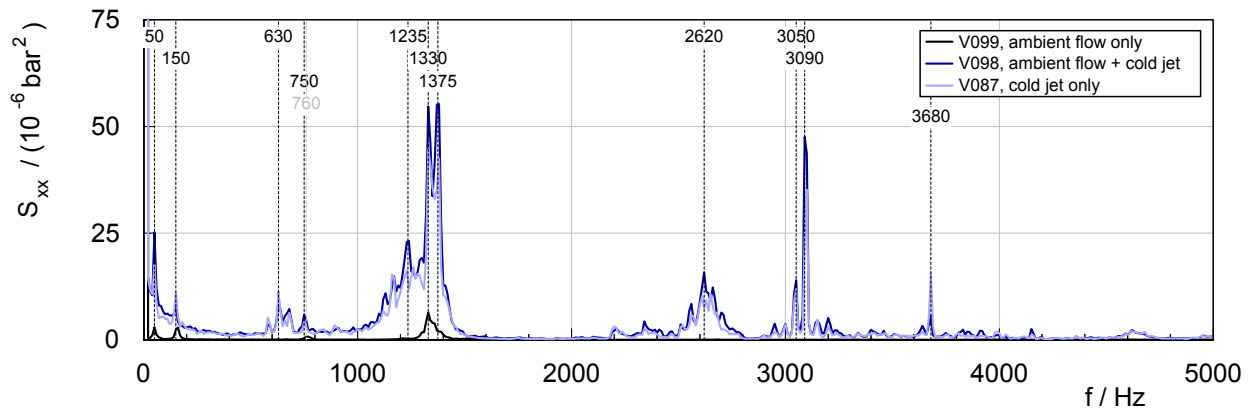
Figure 10: Power spectrum of the combustion chamber pressure signals for the ambient flow case with cold jet (V098); the ambient flow without jet (V099) and jet only (V087) cases are plotted for comparison
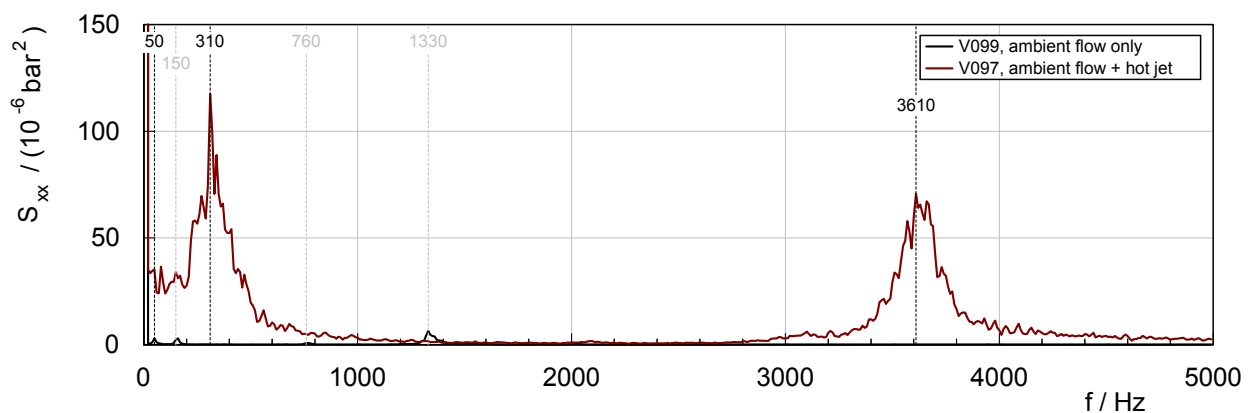
Figure 11: Power spectrum of the combustion chamber pressure signals for the ambient flow case with hot jet (V097); the ambient flow case without jet (V099) is plotted for comparison
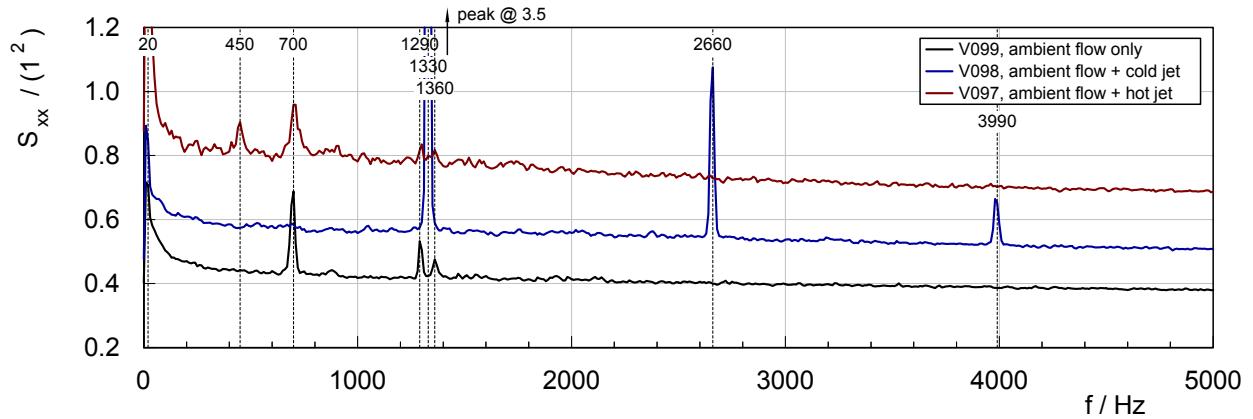
Figure 12: Power spectrum of the intensity fluctuations from the HSS images; amplitude spectra spatially averaged over all pixel locations

convergent nozzle section. In the higher frequency range, additional content is visible around 2620 Hz, 3090 Hz, and 3680 Hz. These were not expected to be linked to the spatial chamber modes, since 2620 Hz would correspond to the 4L mode, whereas the 3L mode is not apparent. They were assumed to be resulting from the injector geometry, but not investigated further. Tangential and radial modes are not visible, since they are lying outside of the resolved frequency range as estimated in Tab. 3.

Adding ambient flow to the isolated cold jet gives very similar results, which is expected since the nozzle flow is supersonic. Nevertheless, at certain frequencies, the amplitude is amplified in case of an interacting flow field. In particular, this is true for the peaks at 1330 Hz and 1375 Hz, where the swinging motion is observed for the ambient flow without jet, as well as for the peak at 750 Hz. In the preceding paragraph, the latter was assigned to the cross-flapping motion. Finally, the power spectrum is also increased at 1235 Hz, which is close to the estimated jet screeching frequency f_{sc} = 1247 Hz. Assuming cross-talk-possibility from the ambient flow to the chamber via the subsonic boundary layer, those findings would give a first hint for a coupling of the broadband 1L and 2L modes of the chamber with the outer flow dynamics.

Investigating the HSS intensity spectrum of the cold jet interaction case (Fig. 12), this hypothesis is emphasized by an extreme peak at around 1330 Hz, which again fits to the swinging motion frequency at f_{sw} = 1318 Hz as well as the 2L mode at f_{2L} = 1313 Hz. Moreover, it is also detected in the power spectrum at 1330 Hz. Further, these peaks appear up to its 4th harmonic frequency at 6640 Hz (only 1st and 2nd printed). This gives rise to the assumption that a strong coupling exists between the broadband chamber pressure oscillations around 1330 Hz, including the 2L mode and the screeching frequency, and the swinging motion of the shear layer. What is unclear at this point is to which extent the three different frequencies contribute to the observed amplification.

Ambient flow with hot jet For the ambient flow with hot jet, the power spectrum of the combustion chamber pressure signal is given in Fig. 11, again in combination with the spectrum for the ambient flow without jet. Here, no narrow-band excitation is visible in the range of the flow or jet dynamics at approximately 760 Hz and 1330 Hz. The spectrum is dominated by two broadband peaks at 310 Hz and 3610 Hz whereas the latter might indicate the first longitudinal mode f_{1L} = 3433 Hz. The difference for the longitudinal mode frequency of about 180 Hz might be due to an inhomogeneous temperature distribution inside the chamber, since the combustion temperature is much higher, than the estimated average temperature from one-dimensional calculations. A radial distribution of the temperature, which is present because of the single element coaxial injector, leads to a faster propagation of pressure waves in the core of the chamber volume. The second peak at 310 Hz cannot be explained by the frequency estimation given in Tab. 3. It is assumed, that the source is designated to the supply infrastructure as already stated in previous work.[4]

The power spectrum of the HSS intensity fluctuations does not reveal increased peaks referred to chamber oscillations. This means that no distinct excitation of the near-wake flow takes place due to fluctuations in the chamber. Nevertheless, peaks can be detected at the same characteristic frequencies as found for the ambient flow without jet (700 Hz, 1290 Hz, and 1360 Hz). Therefore, the flow field is dominated by the well-known near-wake flow dynamics such as the cross-flapping and swinging motion, but without the previously found strong excitation mechanisms and without presumable coupling phenomena. Another peak can be found at 450 Hz. It corresponds to Sr_D = 0.12, but is not directly comparable to the estimated frequencies.

(a) $f_{\text{iso}} = 700\,Hz$ (b) $f_{\text{iso}} = 1290\,Hz$
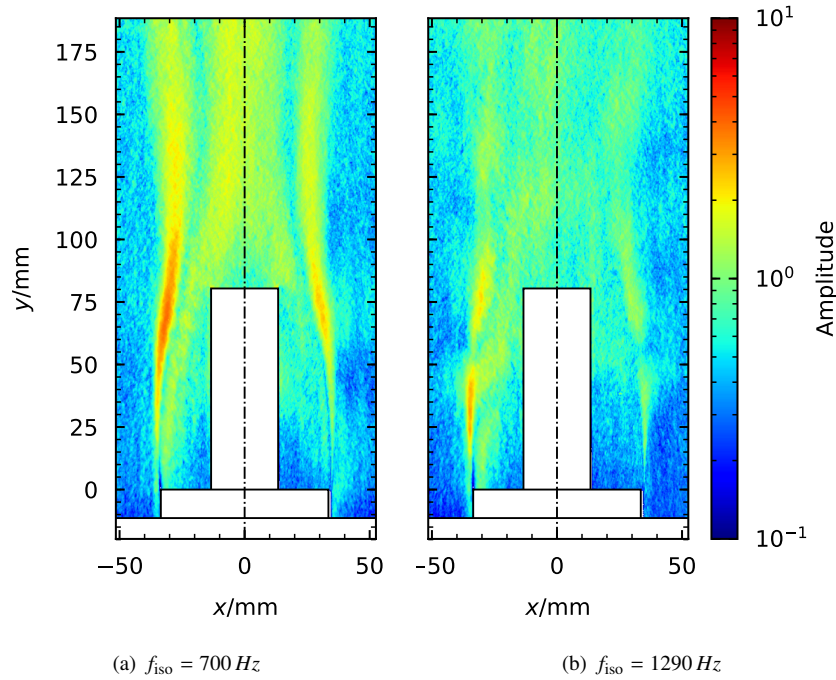
Figure 13: Isolated frequency amplitude distribution of the power spectrum for ambient flow without jet (V099)

3.3 Spatial Distribution of the Dominant Isolated Frequencies

In Section 3.2, various spectral features of the chamber pressure and HSS intensity fluctuations for the different configurations are assigned to the characteristic wake flow modes, as determined in Section 2.5. Although, the agreement with the prediction is remarkable for some frequencies, deviations occur. Thus, final statements can neither be given solely by the assessment of the power spectra, nor the field averaged intensity fluctuations from HSS images, since only the temporal characteristics of the flow field are characterized so far. To finally evaluate the distinctive features of the spectra, they should also be linked to a spatial characteristic or mode of the flow fields motion. This is done in the following section by analyzing the spatial distribution of the amplitude of isolated frequencies in the wake flow field.

Ambient flow without jet   For the ambient flow without jet, the two most dominant frequencies, 700 Hz and 1290 Hz, corresponding to the non-dimensional frequencies of $\text{Sr}_D = 0.19$ and $\text{Sr}_D = 0.34$, respectively, are plotted in Fig. 13 as two-dimensional field of the power spectrum amplitude. They correspond to the peaks found in the spatial average of the power spectra (Fig. 12). In both cases, it is obvious, that the higher amplitudes, which lead to the peak in the average power spectrum are located in the ambient shear layer as well as the wake of the nozzle in which the circular shear layer can interact with itself. Further, for the 700 Hz, the peak amplitudes are found near the nozzle tip in a slim axially elongated region, which is an indication for lateral fluctuations at that place. The same is true for the 1290 Hz distribution, except that the peak region is now split in two sections, which, assuming a 180° phase shift between the two section would result in a swinging motion in the cross direction. Comparing these topologies with the results of the modal decomposition by Statnikov et al. (2017)[10] and Saile (2019),[5] the evidence is that the identified spectra at 700 Hz and 1290 Hz can indeed be characterized as the cross-flapping motion and swinging-motion of the shear layer.

Ambient flow with hot jet   As expected from the average HSS power spectra, the ambient flow case with hot jet interaction behaves similarly to the ambient flow without jet regarding the frequencies of the cross-flapping and swinging motion. In Fig. 14, they are plotted in their most intensified bands, which are 710 Hz for the cross-flapping motion and 1300 Hz for the swinging motion, which corresponds to $\text{Sr}_D = 0.19$ and $\text{Sr}_D = 0.35$. Compared to the ambient flow without jet, the mean amplitude is increased in the whole interacting flow regime. In particular, is true inside the jet and in the far wake of the bluff body, where the shear layers are interacting strongly, but also the recirculation itself experiences larger fluctuations. Note that the Schlieren technique is an integrating method and that fluctuations from the shear layers parallel to the coordinate plane inevitably contribute to the illustrated quantities. In addition to the cross-flapping and swinging motion frequencies, the 450 Hz peak from the average HSS power spectrum is plotted in Fig. 14(a). From a topological point of view, the resulting field is quite similar to that at 710 Hz. The mean amplitude

(a) $f_{\text{iso}} = 450\,Hz$ (b) $f_{\text{iso}} = 710\,Hz$ (c) $f_{\text{iso}} = 1300\,Hz$
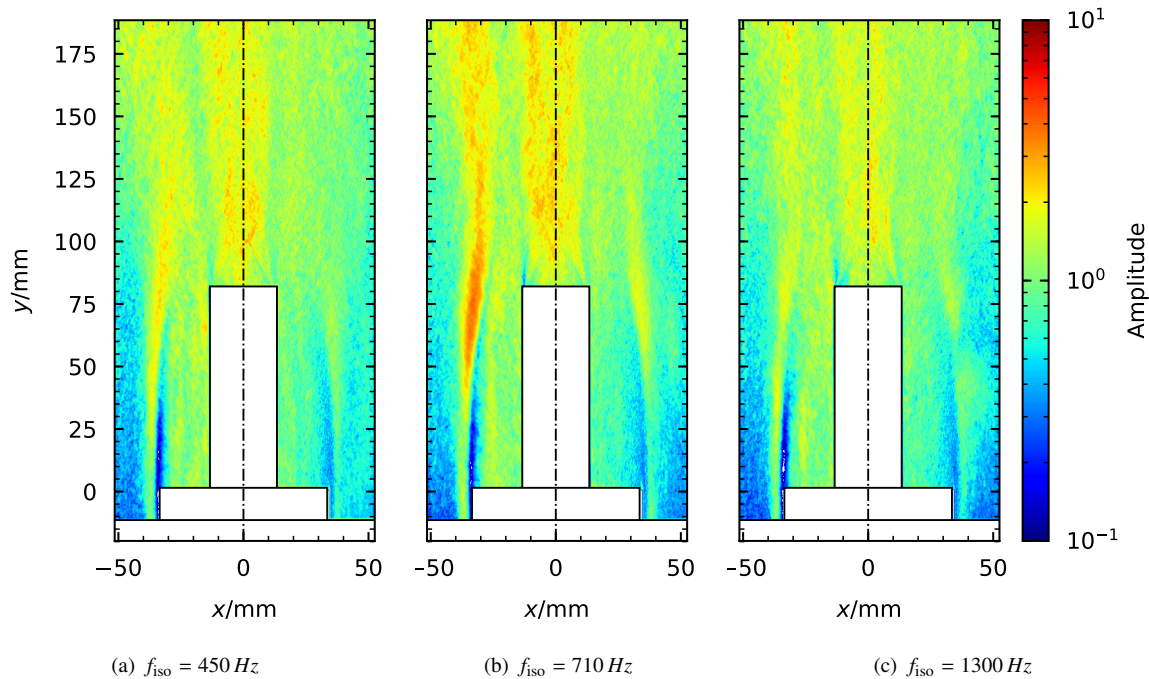
Figure 14: Isolated frequency amplitude distribution of the power spectrum for ambient flow with hot jet (V097)

is somewhat lower and the increase of the amplitudes in the shear layer is not significant. This mode looks more like a global amplification of the vortex structures, leading to local density gradients, that are captured by the analysis. Such amplification could result from other excitation mechanisms, which are not investigated by the chamber pressure and HSS spectra, e. g. a modification of the incoming boundary layer through vibrations of the wind tunnel model or an interaction with the external shear layer of the wind tunnel nozzle.

Ambient flow with cold jet   The three most intensified frequencies (1330 Hz, 2660 Hz, and 3990 Hz) from the HSS power spectrum for the ambient flow case with cold jet interaction are plotted in Fig. 15. From the preceding results, they were described as a coupling of the swinging-motion frequency with the first and second longitudinal mode of the pressure chamber and optionally the screeching frequency.

It can be seen in Fig. 15(a) that the extreme peak at 1330 Hz in the average HSS spectrum indeed comes from a zonal increase of the fluctuation amplitude, rather than a global homogeneous increase of the mean fluctuation. Most of the fluctuation energy is concentrated in circular structures, emanating from the base shoulder and continuing within the shear layer into the far wake. The dimension of those clusters of increased amplitude is growing in the stream-wise direction and their location seems to be about symmetrical along the center axis. Interpreting the findings under the assumption of a generally lateral cross movement of the density gradient field at the location of those clusters, the locations between the clusters with negligible amplitude are identified as stationary nodes of a swinging motion of the shear layer. What is left for a final characterization of the flow motion in the future is the phase information, specifying the temporal relation between the opposite shear layers, which is vital for the characterization of the resulting side loads on the nozzle structure. Note that this excitation was already elaborated in Saile[5,7–9] by means of PIV and pressure measurements. There it is seen as aeroacoustic coupling mechanism between the swinging motion and jet screeching.

Next to the swinging motion of the shear layer, an increase of fluctuation amplitudes is also visible within the jet shear layer, with a significant extent developing downstream of the first Mach disc. Although not fully visible, the structure, which is similarly elongated in the stream-wise direction within the jet shear layer, seems to be repeating at $y = 175\,mm$ and showing the same characteristics as the ambient shear layer. The origin of this phenomenon is seen in the wake flow, imposing a periodically fluctuating pressure field on the supersonic jet, which itself is consequently subjected to a swinging motion. While the first shock cell is still quiet stable, the swinging motion is potentially increasing in the stream-wise direction since both, the effect of the wake flow field as well as the intrinsic disturbances within the jet shear layer should grow while propagating downstream.

Finally, looking on Fig. 15(b) and 15(c), the clustered structure is still visible in the ambient shear layer, while the dimension of each cluster is reduced by about half for each of the higher harmonics. This is also an indicator for a truly periodic movement at 1330 Hz. The higher harmonics are though less prominent in the far wake and in the jet.

13

SPECTRAL ANALYSIS OF ROCKET WAKE FLOW–JET INTERACTION

(a) $f_{\text{iso}} = 1330\,Hz$

(b) $f_{\text{iso}} = 2660\,Hz$

(c) $f_{\text{iso}} = 3990\,Hz$
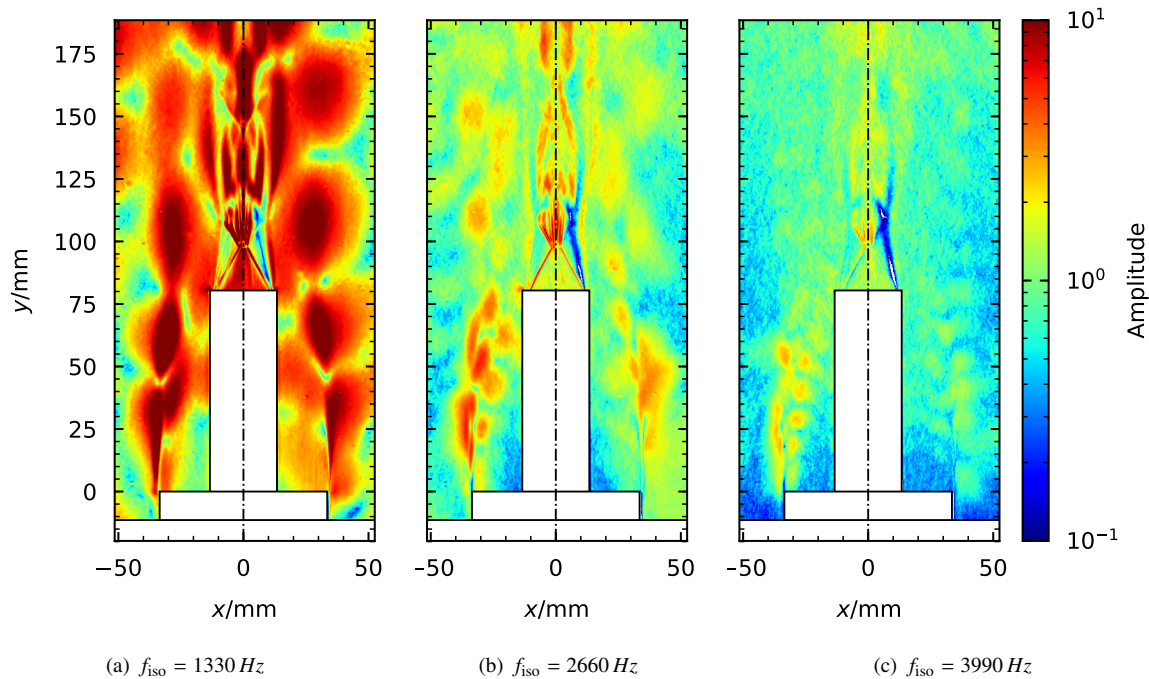
Figure 15: Isolated frequency amplitude distribution of the power spectrum for ambient flow with cold jet (V098)

4. Conclusion and Outlook

Spectral analyzes of the wake flow of a generic rocket launcher geometry at flow Mach number 0.8, interacting with a supersonic exhaust jet by means of HSS imaging revealed large differences in the fluctuating density gradient field between flow configurations with cold or hot exhaust jet. The hot exhaust jet was generated by means of GH2/GO2 combustion inside the wind tunnel model combustion chamber, which is rather unique for base flow investigations. Analytical estimations of the acoustic properties of the pressure chamber, the characteristic wake flow modes, and the dynamic features of the supersonic jet were compared with spectral analyzes of the HSS intensity fluctuations of the near-wake and the total chamber pressure measurements. The objective was to evaluate the remarkable features of the near-wake dynamics with respect to their driving mechanisms.

The cases of ambient flow without jet and ambient flow with hot jet showed the typical wake flow modes, which were in good agreement with the estimated non-dimensional frequencies from literature, such as Statnikov et al. (2017.)[10] The same appeared to be true for the distribution of density gradient fluctuations, which were very similar to the results of Statnikov et al. (2017) with respect to the form and location of the excited areas. The cross-flapping motion was measured at 700 Hz/710 Hz ($\text{Sr}_D = 0.19$) for the cases without jet and with hot jet respectively. The swinging motion was detected in the range of 1290 Hz ($\text{Sr}_D = 0.34$) and 1360Hz ($\text{Sr}_D = 0.36$). The chamber pressure measurements of ambient flow without jet showed peaks in the same regions with a slight frequency shift (760 Hz for the cross-flapping motion), which qualitatively validates the HSS analysis. Additional pressure measurements in the base could enable a final quantitative characterization in future tests.

The ambient flow case with cold exhaust jet showed a resonance peak at 1330 Hz ($\text{Sr}_D = 0.35$) in the spatially averaged spectrum of the HSS intensity fluctuations. The resonance frequency corresponds both, to the estimated swinging motion frequency of the ambient shear layer and the second longitudinal mode (2L) of the pressure chamber, which was also identified in the chamber pressure measurements. The characteristics of the swinging motion were identified by the shape and location of the spatially distributed amplitude of its isolated frequency. Its amplification appears to be more emphasized for the cold than for the hot jet case. However, it must be kept in mind that the scale of the density gradient is strongly dependent on the setting. Associating a quantitative meaning (except for the frequency) is difficult. Finally, it is assumed that a strong coupling exists between the swinging motion of the ambient shear layer and the fluctuating jet shear layer due to the measured chamber pressure fluctuations at its second longitudinal mode.

This deviates from the hypothesis in Saile (2019).[5] There, the same extraordinary excitation is found in the near-wake for a configuration with cold jet and an ambient flow at Mach 0.8 However, it is suggested that jet screech instead of chamber instabilities is the driving mechanism for the amplification of the wake flow modes. For the present study, the estimated screeching frequencies for the cold and hot jet cases (1247 Hz/1330 Hz) were lying close to the

amplified band of the HSS fluctuations and, consequently, to the swinging motion frequency of the ambient shear layer. But, since it was not isolated from the acoustic modes of the pressure chamber for the cold jet case, it is still unclear, which contribution it makes to the observed amplification. Here, the data from the hot jet tests could be consulted for clarification. In this configuration, no such strong amplification of the swinging motion existed, although, the swinging motion and jet screeching frequencies matched perfectly.

Another explanation might be, that the reattachment of the ambient shear layer is not clearly defined for the hot jet case. Saile et al. (2019)[5,9] finds a strong dependency between the shear layer reattachment location and the excitation of the near-wake flow. For the case at hand, the averaged Schlieren images indicated a reattachment farther downstream on the jet, but not on the solid nozzle wall. This might cause a dampening of the vortex shedding mechanism and its corresponding excitation as seen in Saile et al. (2019).[5,9]

Unfortunately, the Schlieren recordings could not capture the reattachment location precisely. Consequently, further studies are suggested to evaluate the reattachment length and to address the sensitivity of the observed excitation with respect to the reattachment of the ambient shear layer. This could be done by modifying the length of the thrust nozzle. Further, to separate the various influences, it is suggested to shift the chamber frequency to a different frequency range, e.g. by modifying the internal chamber geometry. Thus, the different contributions, either of the acoustic chamber modes or the dynamics of the supersonic jet to the excitation of the wake flow modes, could be considered separately.

5. Acknowledgments

References

[1] Fred S. Blomshield. Lessons Learned In Solid Rocket Combustion Instability. In *43rd AIAA/ASME/SAE/ASEE Joint Propulsion Conference & Exhibit*, Cincinnati, Ohio, 8–11 July 2007.

[2] S. David and S. Radulovic. Prediction of Buffet Loads on the Ariane 5 Afterbody. In *6th International Symposium on Launcher Technologies*, Munich, Germany, November 2005.

[3] Oskar J. Haidn, Nikolaus A. Adams, Thomas Sattelmlayer, Christian Stemmer, Rolf Radespiel, Wolfgang Schröder, and Bernhard Weigand. Fundamental Technologies for the Development of Future Space Transportsystem Components under high Thermal and Mechanical Loads. In *2018 Joint Propulsion Conference*, Cincinnati, Ohio, 9–11 July 2018. AIAA 2018-4466.

[4] Daniel Kirchheck and Ali Gülhan. Characterization of a GH2/GO2 Combustor for Hot Plume Wind Tunnel Testing. In *Sonderforschungsbereich/Transregio 40 – Annual Report*. 2018.

[5] Dominik Saile. *Experimental Analysis on Near-Wake Flows of Space Transportation Systems*. PhD thesis, Rheinisch-Westfälische Technische Hochschule (RWTH) Aachen. Submitted in February 2019.

[6] Dominik Saile, Daniel Kirchheck, Ali Gülhan, Chadi Serhan, and Volker Hannemann. Design of a GH2/GOX Combustion Chamber for the Hot Plume Interaction Experiments at DLR Cologne. In *8th European Symposium on Aerothermodynamics for Space Vehicles (ATD)*, Lisbon, Portugal, 2–6 March 2015.

[7] Dominik Saile, Viktor Kühl, and Ali Gülhan. On the subsonic near-wake of a space launcher configuration with jet. *Experiments in Fluids*. Submitted and considered for publication after revision in April 2019.

[8] Dominik Saile, Viktor Kühl, and Ali Gülhan. On the subsonic near-wake of a space launcher configuration without jet. *Experiments in Fluids*, 60(4):50, March 2019.

[9] Dominik Saile, Viktor Kühl, and Ali Gülhan. On Subsonic Near-Wake Flows of Various Base Geometries. In *13th International Symposium on Particle Image Velocimetry (ISPIV)*, Munich, Germany, 22–24 July 2019.

[10] Vladimir Statnikov, Matthias Meinke, and Wolfgang Schröder. Reduced-order analysis of buffet flow of space launchers. *Journal of Fluid Mechanics*, 815:1–25, March 2017.

[11] Sören Stephan and Rolf Radespiel. Propulsive Jet Simulation with Air and Helium in Launcher Wake Flows. *CEAS Space Journal*, 9(2):195–209, 2017.